COMPDYN 2011
III ECCOMAS Thematic Conference on
Computational Methods in Structural Dynamics and Earthquake Engineering
M. Papadrakakis, M. Fragiadakis, V. Plevris (eds.)
Corfu, Greece, 25–28 May 2011

IMPLEMENTATION OF FRACTURE MECHANICS CONCEPTS IN DYNAMIC PROGRESSIVE COLLAPSE PREDICTION USING AN OPTIMIZATION BASED ALGORITHM

David Tubul[1], **and Oren Lavan**[2]
[1]Technion-Israel institute of Technology
Haifa 32000, Israel
e-mail: tubul@tx.technion.ac.il
[2]Technion-Israel institute of Technology
Haifa 32000, Israel
e-mail: lavan@tx.technion.ac.il

Keywords: Progressive collapse, disproportionate collapse, Lagrangian dynamics, Fracture, Strength degradation, Mixed Lagrangian Formulation (MLF).

Abstract. *Prediction of progressive collapse of buildings under extreme events is one of the challenges that the civil engineering community must face. The ability to predict progressive collapse would enable the identification of deficiencies in the common practice of structural design without having to wait for the next extreme event to occur. With such ability, new design strategies and technologies for progressive collapse prevention could be addressed.*

Progressive collapse prediction, where the capacity of structures for progressive collapse is assessed, faces a great number of challenges. In terms of feasibility, it should address the challenge of analyzing large scale buildings in all stages of collapse. The complex behavior of buildings during collapse often leads to issues of stability of the numerical scheme, hence to the collapse of the analysis prior to the actual analysis of collapse. Indeed, the area of dynamics of structures including phenomena expected during progressive collapse (e.g. contact, fracture) has been developed to a high level. Nevertheless, there is no theory and computational tool that can efficiently predict all stages of progressive collapse of large scale structures.

The Mixed Lagrangian Formulation (MLF) could potentially provide such a theory as well as an accompanied efficient, robust and stable numerical scheme. It also considers almost all stages of collapse in a unified manner, thus, almost completes the puzzle of Progressive collapse prediction. The missing part of the puzzle, considering fracture in a unified manner, is the aim of this paper. This is developed using concepts from Fracture Mechanics for brittle material by using Griffith's theory. This, in turn, will lay the foundation for considering more complex models in the future. Additional state variables required to model fracture using fracture mechanics concepts are identified. Subsequently, appropriate stored energy and dissipation functions, which lead to Griffith's theory, are formulated. Once the stored energy and dissipation functions are formulated, Hamilton's principle is discretized in time to lead to an optimization problem at each time step. The solution of the optimization problem supplies with the states at the end of the time step. This results in a sound theory as well as an efficient, robust and stable numerical scheme for progressive collapse prediction, as supported by the examples.

1 INTRODUCTION

Prediction of progressive collapse of large scale buildings due to natural or man-made extreme events is a major challenge in structural engineering. The main challenge stems from the various complex and sudden phenomena that structures experience during collapse. Those often lead to the collapse of the analysis prior to the actual analysis of collapse. With theory and tools for Progressive Collapse Prediction (PCP), deficiencies in the common practice of structural design, in the context of progressive collapse, could be identified without having to wait for the next extreme event to occur. With such theory and tools, the efficiency of existing design strategies for progressive collapse prevention (e.g. [1] and references therein) could be rigorously assessed, and the development of new strategies and technologies could be addressed. In addition, those tools could be used in forensic engineering or for the design of demolition.

The progressive collapse of the Ronan Point apartment building (England, 1968) and the terrorist attacks on the Murrah building (Oklahoma, 1995) and the WTC (New-York city, 2001) revealed the drawbacks of the traditional philosophy behind the design of structures: Buildings are designed to withstand the expected loads with a given performance level, while their capacity to withstand collapse due to extreme events remains unknown. This recognition has led to the new field of PCP in structural engineering. This field addresses the modeling and simulation of buildings up to the prediction of total collapse, where a progressive creation of "rubble" of structural mass is expected. This can be initiated by a rather local damage in a limited number of structural components. This local damage eventually causes a sequential failure of additional components, or a chain reaction, up to collapse. Several phases of behavior can be identified during the progress of collapse. These are elastic behavior, plastic behavior, stiffness and strength degradation, buckling and other geometric nonlinear phenomena, fracture, detachment of objects from the structure and impact or contact of structural elements with each other.

Pretlov et al. [2] pointed out that static analysis cannot capture important effects in progressive collapse. This statement has been verified in numerous occasions (e.g. [3, 4] and references therein). Hence, a dynamic approach should be considered. Here, the modeling for prediction of progressive collapse can be done at several levels. At the finest level, one can adopt micro-modeling, where each of the structural components (beams, columns, etc.) is modeled by a large number of solid elements. The Finite Elements Method (e.g. [5]) or the Distinct Element Method (e.g. [6]) have been adopted in that context. At the other limit, macro-modeling of large structural systems, each story or even the whole structure can be used (e.g. [7, 8]). Recently, an intermediate approach seems to gain attention in the context of PCP. This approach makes use of macro-modeling of different structural components (e.g. [3, 9, 10, 11 ,12 ,13 ,14]). It combines advantages from the two previous approaches as it is general enough to be used for a large spectrum of types of buildings, collapse modes and extreme events, while is potentially feasible for large scale structures. Another advanced approach combines various scales of elements and is based on multibody models [15]. This efficient approach was used for the simulation of collapse considering uncertainty, where a large number of deterministic analyses is required.

A crucial issue in most approaches presented above is the time integration schemes they adopt. The theoretical basis of those methods cannot provide answers regarding the existence or uniqueness of the solutions. Those may be very important in PCP as the complex behavior may lead to bifurcations where more than a single solution may exist. In addition, those numerical schemes require very small time steps. This is due to the sudden changes in the response of structures expected when fracture or contact occur. In case where those numerical

schemes do converge to a solution, it is also not clear whether it is the true physical solution of the problem. If the problem does possess bifurcations, it is not clear what solution those schemes would follow. Additionally, no approach seems to efficiently cover all stages of progressive collapse and enable a feasible prediction for large scale structures.

A new approach for nonlinear dynamic structural analysis, namely the Mixed Lagrangian Formulation (MLF), has recently been proposed [16]. MLF was originally developed for the analysis of elastic-plastic response while considering geometric nonlinearity. This approach lays on a sound theory that may enable the investigation of existence and uniqueness of solutions. It is based on time discretization of Hamilton's principle [17]. Hence, the computation of the response quantities in each time step reduces to the solution of an optimization problem. This weak formulation in time leads to a very stable and accurate numerical scheme that allows for large time step sizes, while allowing for sharp changes in its variables. It also requires a small number of iterations within each time step. In much similarity to the generalized standard material framework [18], MLF is also based on two scalar functions: The stored energy function and the dissipation function.

MLF has been modified to enable an efficient analysis of large scale 3D buildings [19]. It was shown to scale very well with the size of the system analyzed. The theory of MLF and the numerical tool have been successfully extended to account for contact analysis by a carefull formulation of an appropriate stored energy function [20]. The capabilities of this framework have been also extended to account for strength degradation and fracture [21]. This was achieved, however, by somewhat deviating from the rigorous MLF and formulating a new hybrid implicit-explicit approach. MLF can potentially present a unified approach with a strong theoretical background that accounts for all stages of collapse. A more unified approach to include fracture in MLF, which is the aim of this paper, is the missing part of this puzzle.

Development of such a strong theory that includes all stages of collapse in a unified manner would possibly enable finding the answers to some very important questions regarding existence of solutions, their uniqueness, and the sensitivity to perturbations. In addition, the numerical schemes stemming from such theory could be provided with assurance regarding their convergence and the quality of their numerical solutions. Those numerical simulation tools are expected to be efficient, robust and stable while efficiently analyzing large scale structures for all stages of collapse.

The purpose of this paper is to lay the foundations for accounting for fracture in MLF. The analysis of large scale structures in all stages of collapse requires a focus on the scale of the structural elements (beams, columns, etc.). Thus, macro-modeling is used to avoid infeasible computational effort. In this paper, a uni-dimensional brittle element is formulated. This lays the foundations to account for fracture in MLF. Formulations of more complex macro-elements and behavior could then follow, in future research. For that purpose, additional state variables are first identified and added to the formulation. In turn, appropriate Lagrangian and Dissipation functions are formulated. Those are then used with a discretized version of Hamilton's principal to result an optimization problem in each time step. The solution of the optimization problem leads to the values of the state variables at the end of the time step.

2 PROPOSED FORMULATION

In this section it will be shown that appropriate Lagrangian and Dissipation functions could be formulated such that upon their use with the Euler-Lagrange equations, the known governing equations could be attained. The proposed Lagrangian and Dissipation functions would be used in the next section to form a robust numerical scheme. In order to present the concept of

the proposed formulation the simplest case of a SDOF system with equal damage in tension and compression will be considered first. More general cases will then follow.

As discussed above, macro-modeling is used to avoid infeasible computational effort. At this stage of research, a uni-dimensional brittle element is formulated to lay the foundations to account for fracture in MLF. Being an energy based approach, MLF could strongly benefit from adopting energy based criteria for fracture. A well-known criterion for fracture of brittle materials, for example, is based on Griffith's theory (e.g. [22, 23]). This criterion states that a crack would propagate if the energy to be released by the incremental growth of the crack, or energy release rate, is larger than the surface energy of the material. This criterion is incorporated to MLF by adopting the crack area as an additional state variable in MLF. In turn, appropriate Lagrangian and Dissipation functions are carefully formulated. It should be noted that as the purpose of this paper is to lay the foundations for incorporating fracture and damage mechanics concepts in MLF, Griffith's theory is applied here to model damage in both tension and compression.

2.1 SDOF system with equal damage in tension and compression

In order to account for fracture, this section makes use of a uni-dimensional macro-element whose stiffness in both tension and compression depends on a "crack area" variable, a. Modifications will be done in the following sections to account for different behavior in tension and compression and MDOF systems.

Let us consider the SDOF system presented in Figure 1. It is comprised of a mass, m, a dashpot having a damping coefficient c and a spring whose stiffness $k(a)$ depends on a "crack area" variable, a, in an appropriate manner. Let us also assume that the evolution of the crack propagation obeys Griffith's theory. The aim of this section is to formulate appropriate Lagrangian and Dissipation function such that upon their substitution to Euler-Lagrange equations one could attain the known governing equations (the equilibrium equation and an equation to reflect Griffith's theory)

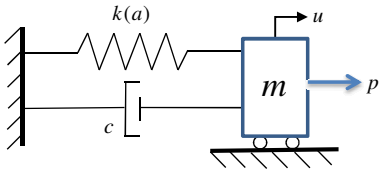

Figure 1: SDOF system with equal damage in tension and compression.

The proposed Lagrangian and Dissipation functions take the form:

$$L(u,\dot{u},a) = \frac{1}{2}m\dot{u}^2 - \frac{1}{2}\cdot k(a)\cdot u^2 + p^T u - g(a) \tag{1}$$

$$\bar{\varphi}(\dot{u},\dot{a}) = \frac{1}{2}c\dot{u}^2 + \varphi(\dot{a}) + 2\gamma\dot{a} \tag{2}$$

Where L is the Lagrangian function, $\bar{\varphi}$ is the Dissipation function, m is the mass of the system, c is the damping coefficient of the dashpot, $k(a)$ is the stiffness of the spring , a is the fracture area or damage parameter, $u(t)$ is the displacement of the mass, γ is the surface energy, $p(t)$ is the external force exerted on the mass, t is time, a dot represents a derivative w.r.t time and $\varphi(\cdot)$ and $g(\cdot)$ convex index functions. Figure 2a presents the function $g(\cdot)$ and Figure 2c

presents the function $\varphi(\cdot)$. In these figures a_0 is the total cross section area. Their derivatives $\partial g(a)/\partial a$ and $\partial\varphi(\dot{a})/\partial\dot{a}$ are presented in Figures 2b and 2d, respectively. Those will be used later on. As can be seen, the function $g(\cdot)$ is zero for values of $a<a_0$ and can take any positive value when $a=a_0$. This will later lead to a constraint on a such that $a\leq a_0$. The function $\varphi(\cdot)$, on the other hand, is assigned with a zero value for $\dot{a}>0$ and can take any positive value when $\dot{a}=0$. This will be required for controlling the propagation of fracture.

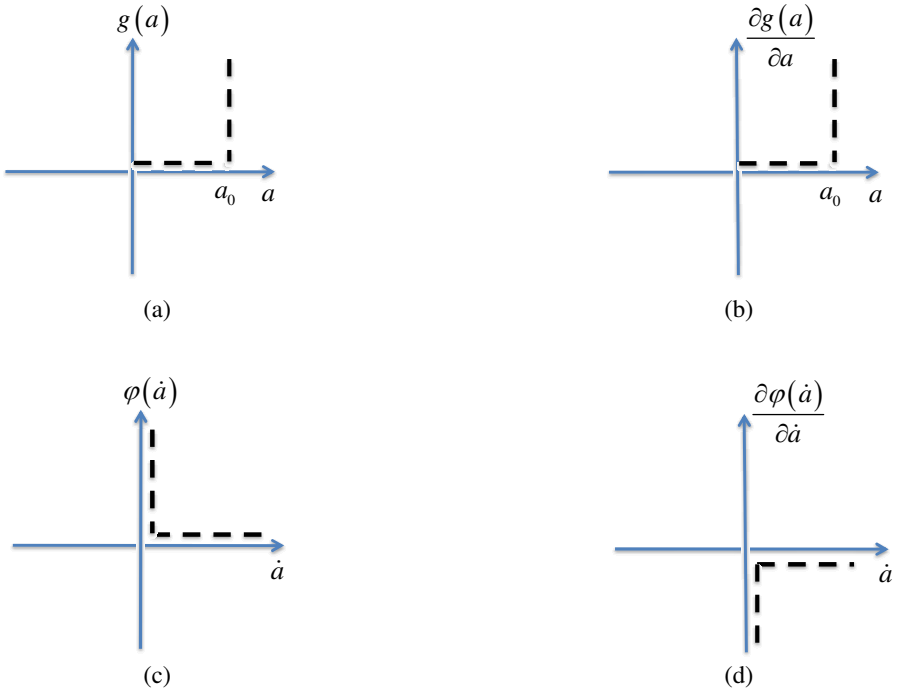

Figure 2: Index functions for the SDOF system with equal damage in tension and compression.

For the problem at hand, with both the displacement and the crack area as state variables, the Euler-Lagrange equations in terms of the Lagrangian and Dissipation functions are given as follows:

$$\frac{d}{dt}\left(\frac{\partial L}{\partial \dot{u}}\right)-\frac{\partial L}{\partial u}+\frac{\partial \overline{\varphi}}{\partial \dot{u}}=0 \tag{3}$$

$$\frac{d}{dt}\left(\frac{\partial L}{\partial \dot{a}}\right)-\frac{\partial L}{\partial a}+\frac{\partial \overline{\varphi}}{\partial \dot{a}}=0 \tag{4}$$

Upon substitution of the proposed Lagrangian and Dissipation functions to the first of Euler-Lagrange equations (Equation 3) one could attain the first governing equation as follows:

$$m\ddot{u}+k(a)\cdot u+c\dot{u}=p \tag{5}$$

This equation is, obviously, the equation of motion of the system. Substitution of the proposed Lagrangian and Dissipation functions to the second of Euler-Lagrange equations (Equation 4) leads to:

$$\frac{1}{2}\frac{\partial k(a)}{\partial a}u^2+\frac{\partial\varphi(\dot{a})}{\partial\dot{a}}+\frac{\partial g(a)}{\partial a}+2\gamma=0 \tag{6}$$

This equation could be brought to the form:

$$-\frac{\partial \Pi}{\partial a}-\frac{\partial \varphi(\dot{a})}{\partial \dot{a}}-\frac{\partial g(a)}{\partial a}=2\gamma \tag{7}$$

where $\Pi=U_E-W$, U_E is the elastic energy and W is the work performed by the applied loads. That is, $-\Pi$ is the complementary energy. This equation controls the crack propagation. It is, actually, equivalent to Griffiths theory where in order to increase the length of the crack the negative of the derivative of the potential energy, $\Pi=U_E-W$, w.r.t the crack length, should be equal to 2γ as will now be demonstrated.

Let us first consider the case where $a<a_0$. In this case, as can be seen from Figure 2b, a value of zero is assigned to $\partial g(a)/\partial a$. Hence, the value of $\partial\varphi(\dot{a})/\partial\dot{a}$ (from Equation 7) depends on the value of $-\partial\Pi/\partial a$ as well as on the value of 2γ. As can be seen by Equation 7, when $-\partial\Pi/\partial a=2\gamma$ (and $a<a_0$) a value of zero is assigned to $\partial\varphi(\dot{a})/\partial\dot{a}$. Hence, from Figure 2d, $\dot{a}$ can be equal or larger than zero and fracture can take place. If, on the contrary, $-\partial\Pi/\partial a<2\gamma$ (and $a<a_0$) a negative value is required for $\partial\varphi(\dot{a})/\partial\dot{a}$ so as to satisfy Equation 7. Hence, from Figure 2d, $\dot{a}=0$ and fracture cannot propagate. The case where $-\partial\Pi/\partial a>2\gamma$ (and $a<a_0$) cannot be attained since in that case fracture already would have occurred earlier.

In the case where $a=a_0$ the spring is fully fractured and fracture can no longer propagate. This is accounted for in the formulation by using the function $g(a)$ that penalizes values of a larger than a_0. This is reflected in Equation 7 as $\partial g(a)/\partial a$ can take any non-negative value (Figure 2b) while $\partial\varphi(\dot{a})/\partial\dot{a}$ can be assigned with any non-positive value. Hence, Equation 7 indicates that fracture can no longer propagate. In this case, the spring loses its stiffness. Although not necessary, the spring could be removed manually at the end of the time step where a reached a_0. Note that fracture (or damage) evolution is enabled by considering the term $\varphi(\cdot)$. Appearing in the Dissipation function, this term leads to an irreversible process. Hence, fracture (or damage) that is created by increase of area crack cannot reduce even if the force is reversed. That is, the crack area variable can only increase.

2.2 SDOF system with different damage in tension and compression

The model presented in the previous section is now extended to account for different behavior in tension and in compression. For that purpose, a tension-only element and a compression-only element are introduced. The former can take only tension forces when the relative displacement at its edges is zero while its internal force is zero when the relative displacement is negative (i.e. the element is shortens). The latter can take only compression forces when the relative displacement at its edges is zero while its internal force is zero when the relative displacement is positive (i.e. the element elongates). The assembly of the system is presented in Figure 3. It is comprised of a mass, a dashpot and two springs in parallel. The first spring is connected in series to a tension-only element while the second spring is connected in series to a compression-only element. Thus, different behavior could be modeled for tension and compression. Both springs are assumed to depend on "crack area" or damage variables. Although Griffith's theory was originally proposed for the propagation of cracks due to tension, both "crack area" variables in tension and in compression are assumed here to evolve obeying Griffith's theory.

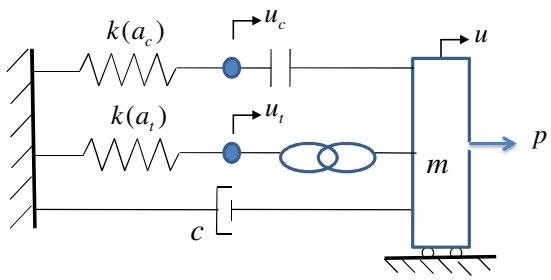

Figure 3: SDOF system with different damage in tension and compression.

The proposed Lagrangian and Dissipation functions take the form:

$$L=\frac{1}{2}m\dot{u}^2-\frac{1}{2}k_t\left(a_t\right)u_t^2-\frac{1}{2}k_c\left(a_c\right)u_c^2-g\left(a_t\right)-g\left(a_c\right)-\eta_t\left(u-u_t\right)-\eta_c\left(u-u_c\right)+pu$$
$$\varphi=\frac{1}{2}c\dot{u}^2+\varphi\left(\dot{a}_t\right)+2\gamma_t\dot{a}_t+\varphi\left(\dot{a}_c\right)+2\gamma_c\dot{a}_c \tag{8}$$

where the subscript t represents variables related to the tension-only system, the subscript c represents variables related to the compression-only system, and the convex functions η_t and η_c are presented in Figure 4 with their partial derivatives w.r.t their arguments. Those functions would later lead to the tension-only and compression-only behavior.

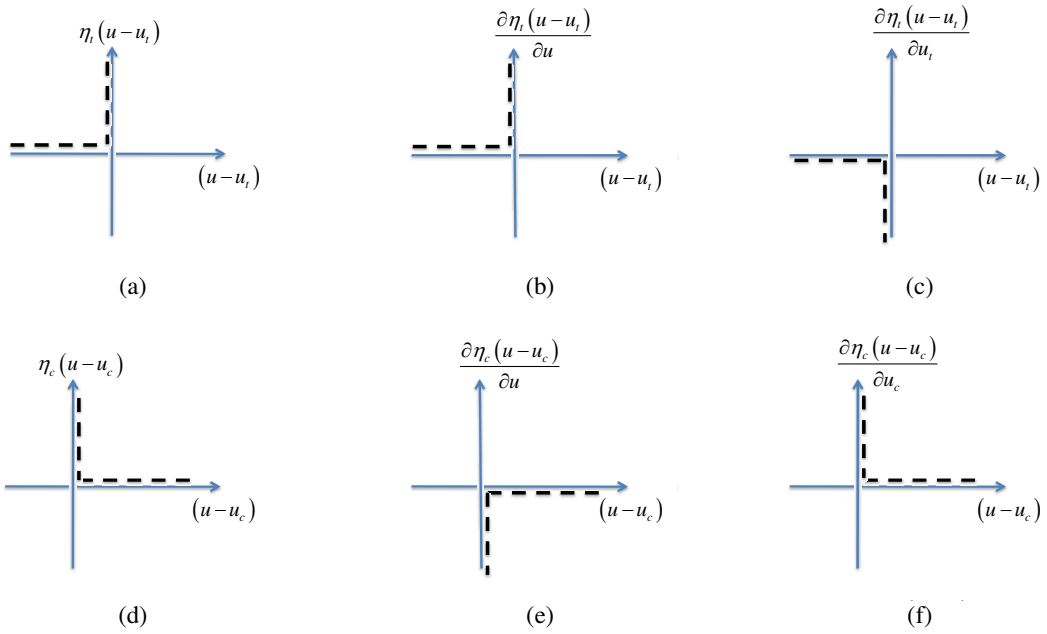

Figure 4: Index functions for the SDOF system with different damage in tension and compression.

For the problem at hand, with the displacements u, u_t and u_c, as well as the "crack area" variables a_t and a_c, as state variables, the Euler-Lagrange equations are given as follows:

$$\begin{cases} u: & m\ddot{u}+\dfrac{\partial \eta_t\left(u-u_t\right)}{\partial u}+\dfrac{\partial \eta_c\left(u-u_c\right)}{\partial u}+c\dot{u}=p \\ u_t: & k_t\left(a_t\right)u_t+\dfrac{\partial \eta_t\left(u-u_t\right)}{\partial u_t}=0 \\ u_c: & k_c\left(a_c\right)u_c+\dfrac{\partial \eta_c\left(u-u_c\right)}{\partial u_c}=0 \\ a_t: & \dfrac{1}{2}\dfrac{\partial k_t\left(a_t\right)}{\partial a_t}u_t^2+\dfrac{\partial g\left(a_t\right)}{\partial a_t}+\dfrac{\partial \varphi\left(\dot{a}_t\right)}{\partial \dot{a}_t}+2\gamma_t=0 \;\rightarrow\; -\dfrac{1}{2}\dfrac{\partial k_t\left(a_t\right)}{\partial a_t}u_t^2-\dfrac{\partial g\left(a_t\right)}{\partial a_t}-\dfrac{\partial \varphi\left(\dot{a}_t\right)}{\partial \dot{a}_t}=2\gamma_t \\ a_c: & \dfrac{1}{2}\dfrac{\partial k_c\left(a_c\right)}{\partial a_c}u_c^2+\dfrac{\partial g\left(a_c\right)}{\partial a_c}+\dfrac{\partial \varphi\left(\dot{a}_c\right)}{\partial \dot{a}_c}+2\gamma_c=0 \;\rightarrow\; -\dfrac{1}{2}\dfrac{\partial k_c\left(a_t\right)}{\partial a_c}u_c^2-\dfrac{\partial g\left(a_c\right)}{\partial a_c}-\dfrac{\partial \varphi\left(\dot{a}_c\right)}{\partial \dot{a}_c}=2\gamma_c \end{cases} \tag{9}$$

Here the first equation is the equation of motion while the fourth and fifth equations dictate the evolution of the "crack area" variables for the tension and compression springs, respectively. The second and third equations enforce tension-only and compression-only behavior on the springs connected to the tension-only and compression-only elements, respectively, as will now be demonstrated.

Let us first note that $\partial \eta_t\left(u-u_t\right)/\partial u=-\partial \eta_t\left(u-u_t\right)/\partial u_t$. Hence, from the second of Equation 9 one could write $\partial \eta_t\left(u-u_t\right)/\partial u=k_t\left(a_t\right)u_t$. That is, in the first of Equation 9 one could replace $\partial \eta_t\left(u-u_t\right)/\partial u$ with $k_t\left(a_t\right)u_t$. Let us now focus on the second of Equation 9 with Figure 4c. As can be seen from Figure 4c, when $u<u_t$ a zero value is assigned to $\partial \eta_t\left(u-u_t\right)/\partial u_t$. Hence, from the second of Equation 9, $k_t\left(a_t\right)u_t=0$ and the spring force is zero. It could also be seen that in that case $u_t=0$ thus $u<0$. If, on the other hand, $u=u_t$, a non-positive value is assigned to $\partial \eta_t\left(u-u_t\right)/\partial u_t$. Hence, from the second of Equation 9, $k_t\left(a_t\right)u_t\geq 0$ and the spring force is non-negative. It could also be seen that in that case $u_t\geq 0$. A similar argument holds for the compression only system.

2.3 MDOF system with contact

The formulation of the previous section is now generalized to MDOF systems. Here, the Lagrangian and Dissipation functions are formulated in terms of vectors representing the displacements of the various degrees-of-freedom (DOFs), $\boldsymbol{u}$, the displacements of the tension-only and compression-only elements, $\boldsymbol{u}_t$ and $\boldsymbol{u}_c$, and the "crack area" variables for the tension-only and compression-only systems, $\boldsymbol{a}_t$ and $\boldsymbol{a}_c$, respectively. The proposed Lagrangian and Dissipation functions take the form:

$$\begin{aligned} L(\boldsymbol{u},\dot{\boldsymbol{u}},\boldsymbol{a})=&\frac{1}{2}\dot{\boldsymbol{u}}^T\mathbf{M}\dot{\boldsymbol{u}}-\frac{1}{2}\boldsymbol{u}_t^T\mathbf{K}_t(\boldsymbol{a}_t)\boldsymbol{u}_t-\frac{1}{2}\boldsymbol{u}_c^T\mathbf{K}_c(\boldsymbol{a}_c)\boldsymbol{u}_c \\ &-g(\boldsymbol{a}_t)-g(\boldsymbol{a}_c)-\eta\left(\boldsymbol{B}^T\boldsymbol{u}-\boldsymbol{u}_t\right)-\eta\left(\boldsymbol{B}^T\boldsymbol{u}-\boldsymbol{u}_c\right)+\boldsymbol{p}^T\boldsymbol{u} \end{aligned} \tag{10}$$

$$\varphi(\dot{\boldsymbol{u}},\dot{\boldsymbol{a}})=\frac{1}{2}\dot{\boldsymbol{u}}^T\mathbf{C}\dot{\boldsymbol{u}}+\varphi\left(\dot{\boldsymbol{a}}_t\right)+2\boldsymbol{\gamma}_t^T\dot{\boldsymbol{a}}+\varphi\left(\dot{\boldsymbol{a}}_c\right)+2\boldsymbol{\gamma}_t^T\dot{\boldsymbol{a}} \tag{11}$$

where $\mathbf{M}$ is the mass matrix, $\mathbf{K}_t$ and $\mathbf{K}_c$ are the stiffness matrices of the tension and the compression springs in their local coordinate systems, respectively, $\boldsymbol{B}^T$ is the compatibility ma-

trix , **C** is the damping matrix , **p** is the external force vector on the DOFs , $\boldsymbol{\gamma}_t$ and $\boldsymbol{\gamma}_c$ are the surface energy vectors (energy threshold values for damage propagation) for the tension and the compression respectively, The scalar functions g, η and φ were defined in previous sections for scalar arguments. In the case of vector arguments the sum of the values attained for each entry of the vector as the argument is taken (e.g. $g(\boldsymbol{a}_t) = g(a_{t,1})+g(a_{t,2})+\cdots+g(a_{t,n})$).

It should be noted that the displacements of the DOFs are sufficient to define the state of all masses. The mass matrix, the damping matrix and the external force vector are defined in this coordinate system. Displacements of additional DOFs, however, are required to define the state of the system. Those are the displacements of the tension-only and compression-only elements. The stiffness matrices are defined in this coordinate system. The functions η, required to account for tension-only and compression-only elements, compare displacements from the two different coordinate systems. Hence, the compatibility matrix, $\boldsymbol{B}^T$, transforms displacements from one coordinate system to the other, is required (can be seen in example 4.2).

As the displacements $\boldsymbol{u}$, $\boldsymbol{u}_t$ and $\boldsymbol{u}_c$, and the "crack area" variables $\boldsymbol{a}_t$ and $\boldsymbol{a}_c$, are adopted here as state variables, the Euler-Lagrange equations take the following form:

$$\begin{cases} \boldsymbol{u}: & \mathbf{M}\ddot{\boldsymbol{u}}+\dfrac{\partial\eta_t\left(\boldsymbol{B}^T\boldsymbol{u}-\boldsymbol{u}_t\right)}{\partial\boldsymbol{u}}+\dfrac{\partial\eta_c\left(\boldsymbol{B}^T\boldsymbol{u}-\boldsymbol{u}_c\right)}{\partial\boldsymbol{u}}+\mathbf{C}\dot{\boldsymbol{u}}=\boldsymbol{p} \\ \boldsymbol{u}_t: & \mathbf{K}_t(\boldsymbol{a}_t)\boldsymbol{u}_t+\dfrac{\partial\eta_t\left(\boldsymbol{B}^T\boldsymbol{u}-\boldsymbol{u}_t\right)}{\partial\boldsymbol{u}_t}=0 \\ \boldsymbol{u}_c: & \mathbf{K}_c(\boldsymbol{a}_c)\boldsymbol{u}_c+\dfrac{\partial\eta_c\left(\boldsymbol{B}^T\boldsymbol{u}-\boldsymbol{u}_c\right)}{\partial\boldsymbol{u}_c}=0 \\ \boldsymbol{a}_t: & \dfrac{1}{2}\boldsymbol{u}_t^T\dfrac{\partial\mathbf{K}_t(\boldsymbol{a}_t)}{\partial\boldsymbol{a}_t}\boldsymbol{u}_t+\dfrac{\partial g\left(\boldsymbol{a}_t\right)}{\partial\boldsymbol{a}_t}+\dfrac{\partial\varphi\left(\dot{\boldsymbol{a}}_t\right)}{\partial\dot{\boldsymbol{a}}_t}+2\boldsymbol{\gamma}_t=0 \\ \boldsymbol{a}_c: & \dfrac{1}{2}\boldsymbol{u}_c^T\dfrac{\partial\mathbf{K}_c(\boldsymbol{a}_c)}{\partial\boldsymbol{a}_c}\boldsymbol{u}_c+\dfrac{\partial g\left(\boldsymbol{a}_c\right)}{\partial\boldsymbol{a}_c}+\dfrac{\partial\varphi\left(\dot{\boldsymbol{a}}_c\right)}{\partial\dot{\boldsymbol{a}}_c}+2\boldsymbol{\gamma}_c=0 \end{cases} \tag{12}$$

As in the previous section, here the first equation is the equation of motion. The second and third equations enforce tension-only and compression-only behavior on the springs connected to the tension-only and compression-only elements, respectively. And the fourth and fifth equations dictate the evolution of the "crack area" variables for the tension and compression springs, respectively.

3 PROPOSED NUMERICAL SCHEME

In the previous section, appropriate Lagrangian and Dissipation functions have been formulated. It was shown that use of those functions with the Euler-Lagrange equations leads to the expected governing equations. Those include the equations of motion as well as the equations for the evolution of the crack area. The traditional approach would make use of advanced time discretization schemes to integrate those equations in time at their strong form. With those Lagrangian and Dissipation functions at hand, however, another approach could be taken using the weak form (in time). That is, those functions could be used with Hamilton's principal. By discretizing the action integral in time, the value of the state variables at the end of the time step may be attained by finding a stationary point of a discrete functional.

In some cases, the stationary point is actually a minimum, hence, an optimization problem could be attained. This leads to a very robust numerical scheme that allows for sharp gradients of the state variables in time. The derivations to follow do not directly apply Hamilton's principal. For the case of an elastic-plastic behavior, however, it was shown [16] that those are equivalent to directly applying Hamilton's principal.

Let us first write Equations 12 at time i+½ using the central difference approximation:

$$
\begin{aligned}
&\mathbf{M}\left(\frac{\boldsymbol{v}_{i+1}-\boldsymbol{v}_i}{h}\right)+\mathbf{C}\left(\frac{\boldsymbol{v}_{i+1}+\boldsymbol{v}_i}{2}\right)+\frac{1}{2}\left[\left.\frac{\partial \eta_t\left(\boldsymbol{B}^T\boldsymbol{u}-\boldsymbol{u}_t\right)}{\partial \boldsymbol{u}}\right|_{i+1}+\left.\frac{\partial \eta_t\left(\boldsymbol{B}^T\boldsymbol{u}-\boldsymbol{u}_t\right)}{\partial \boldsymbol{u}}\right|_{i}\right]\\
&+\frac{1}{2}\left[\left.\frac{\partial \eta_c\left(\boldsymbol{B}^T\boldsymbol{u}-\boldsymbol{u}_c\right)}{\partial \boldsymbol{u}}\right|_{i+1}+\left.\frac{\partial \eta_c\left(\boldsymbol{B}^T\boldsymbol{u}-\boldsymbol{u}_c\right)}{\partial \boldsymbol{u}}\right|_{i}\right]-\frac{\boldsymbol{p}_{i+1}+\boldsymbol{p}_i}{2}=0\\
&\frac{1}{2}\left[\mathbf{K}_t(\boldsymbol{a}_{t,i+1})\boldsymbol{u}_{t,i+1}+\mathbf{K}_t(\boldsymbol{a}_{t,i})\boldsymbol{u}_{t,i}\right]+\frac{1}{2}\left[\left.\frac{\partial \eta_t\left(\boldsymbol{B}^T\boldsymbol{u}-\boldsymbol{u}_t\right)}{\partial \boldsymbol{u}_t}\right|_{i+1}+\left.\frac{\partial \eta_t\left(\boldsymbol{B}^T\boldsymbol{u}-\boldsymbol{u}_t\right)}{\partial \boldsymbol{u}_t}\right|_{i}\right]=0\\
&\frac{1}{2}\left[\mathbf{K}_c(\boldsymbol{a}_{c,i+1})\boldsymbol{u}_{c,i+1}+\mathbf{K}_c(\boldsymbol{a}_{c,i})\boldsymbol{u}_{c,i}\right]+\frac{1}{2}\left[\left.\frac{\partial \eta_c\left(\boldsymbol{B}^T\boldsymbol{u}-\boldsymbol{u}_c\right)}{\partial \boldsymbol{u}_c}\right|_{i+1}+\left.\frac{\partial \eta_c\left(\boldsymbol{B}^T\boldsymbol{u}-\boldsymbol{u}_c\right)}{\partial \boldsymbol{u}_c}\right|_{i}\right]=0\\
&\frac{1}{2}\left[\frac{1}{2}\boldsymbol{u}_{t,i+1}^T\frac{\partial \mathbf{K}_t(\boldsymbol{a}_{t,i+1})}{\partial \boldsymbol{a}_{t,i+1}}\boldsymbol{u}_{t,i+1}+\frac{1}{2}\boldsymbol{u}_{t,i}^T\frac{\partial \mathbf{K}_t(\boldsymbol{a}_{t,i})}{\partial \boldsymbol{a}_{t,i}}\boldsymbol{u}_{t,i}\right]+\frac{1}{2}\left[\left.\frac{\partial g(\boldsymbol{a}_t)}{\partial \boldsymbol{a}_t}\right|_{i+1}+\left.\frac{\partial g(\boldsymbol{a}_t)}{\partial \boldsymbol{a}_t}\right|_{i}\right]+\frac{1}{2}\left[\left.\frac{\partial \varphi(\dot{\boldsymbol{a}}_t)}{\partial \dot{\boldsymbol{a}}_t}\right|_{i+1}+\left.\frac{\partial \varphi(\dot{\boldsymbol{a}}_t)}{\partial \dot{\boldsymbol{a}}_t}\right|_{i}\right]+2\boldsymbol{\gamma}_t=0\\
&\frac{1}{2}\left[\frac{1}{2}\boldsymbol{u}_{c,i+1}^T\frac{\partial \mathbf{K}_c(\boldsymbol{a}_{c,i+1})}{\partial \boldsymbol{a}_{c,i+1}}\boldsymbol{u}_{c,i+1}+\frac{1}{2}\boldsymbol{u}_{c,i}^T\frac{\partial \mathbf{K}_c(\boldsymbol{a}_{c,i})}{\partial \boldsymbol{a}_{c,i}}\boldsymbol{u}_{c,i}\right]+\frac{1}{2}\left[\left.\frac{\partial g(\boldsymbol{a}_c)}{\partial \boldsymbol{a}_c}\right|_{i+1}+\left.\frac{\partial g(\boldsymbol{a}_c)}{\partial \boldsymbol{a}_c}\right|_{i}\right]+\frac{1}{2}\left[\left.\frac{\partial \varphi(\dot{\boldsymbol{a}}_c)}{\partial \dot{\boldsymbol{a}}_c}\right|_{i+1}+\left.\frac{\partial \varphi(\dot{\boldsymbol{a}}_c)}{\partial \dot{\boldsymbol{a}}_c}\right|_{i}\right]+2\boldsymbol{\gamma}_c=0
\end{aligned}
\tag{13}
$$

Using the approximation $\boldsymbol{u}_{j,i+1}=\boldsymbol{u}_{j,i}+\frac{h}{2}\left(\boldsymbol{v}_{j,i+1}+\boldsymbol{v}_{j,i}\right)$ one could obtain:

$$
\begin{aligned}
&\frac{1}{h}\mathbf{M}\boldsymbol{v}_{i+1}-\frac{1}{h}\mathbf{M}\boldsymbol{v}_i+\frac{1}{2}\mathbf{C}\boldsymbol{v}_{i+1}+\frac{1}{2}\mathbf{C}\boldsymbol{v}_i+\frac{1}{2}\left[\left.\frac{\partial \eta_t\left(\boldsymbol{B}^T\boldsymbol{u}-\boldsymbol{u}_t\right)}{\partial \boldsymbol{u}}\right|_{i+1}+\left.\frac{\partial \eta_t\left(\boldsymbol{B}^T\boldsymbol{u}-\boldsymbol{u}_t\right)}{\partial \boldsymbol{u}}\right|_{i}\right]\\
&+\frac{1}{2}\left[\left.\frac{\partial \eta_c\left(\boldsymbol{B}^T\boldsymbol{u}-\boldsymbol{u}_c\right)}{\partial \boldsymbol{u}}\right|_{i+1}+\left.\frac{\partial \eta_c\left(\boldsymbol{B}^T\boldsymbol{u}-\boldsymbol{u}_c\right)}{\partial \boldsymbol{u}}\right|_{i}\right]-\frac{\boldsymbol{p}_{i+1}+\boldsymbol{p}_i}{2}=0\\
&\frac{1}{2}\mathbf{K}_t(\boldsymbol{a}_{t,i+1})\boldsymbol{u}_{t,i}+\frac{h}{4}\mathbf{K}_t(\boldsymbol{a}_{t,i+1})\boldsymbol{v}_{t,i+1}+\frac{h}{4}\mathbf{K}_t(\boldsymbol{a}_{t,i+1})\boldsymbol{v}_{t,i}+\frac{1}{2}\mathbf{K}_t(\boldsymbol{a}_{t,i})\boldsymbol{u}_{t,i}+\frac{1}{2}\left[\left.\frac{\partial \eta_t\left(\boldsymbol{B}^T\boldsymbol{u}-\boldsymbol{u}_t\right)}{\partial \boldsymbol{u}_t}\right|_{i+1}+\left.\frac{\partial \eta_t\left(\boldsymbol{B}^T\boldsymbol{u}-\boldsymbol{u}_t\right)}{\partial \boldsymbol{u}_t}\right|_{i}\right]=0\\
&\frac{1}{2}\mathbf{K}_c(\boldsymbol{a}_{c,i+1})\boldsymbol{u}_{c,i}+\frac{h}{4}\mathbf{K}_c(\boldsymbol{a}_{c,i+1})\boldsymbol{v}_{c,i+1}+\frac{h}{4}\mathbf{K}_c(\boldsymbol{a}_{c,i+1})\boldsymbol{v}_{c,i}+\frac{1}{2}\mathbf{K}_c(\boldsymbol{a}_{c,i})\boldsymbol{u}_{c,i}+\frac{1}{2}\left[\left.\frac{\partial \eta_c\left(\boldsymbol{B}^T\boldsymbol{u}-\boldsymbol{u}_c\right)}{\partial \boldsymbol{u}_c}\right|_{i+1}+\left.\frac{\partial \eta_c\left(\boldsymbol{B}^T\boldsymbol{u}-\boldsymbol{u}_c\right)}{\partial \boldsymbol{u}_c}\right|_{i}\right]=0\\
&\frac{1}{2}\left[\frac{1}{2}\left(\boldsymbol{u}_{t,i}+\frac{h}{2}\left(\boldsymbol{v}_{t,i+1}+\boldsymbol{v}_{t,i}\right)\right)^T\frac{\partial \mathbf{K}_t(\boldsymbol{a}_{t,i+1})}{\partial \boldsymbol{a}_{t,i+1}}\left(\boldsymbol{u}_{t,i}+\frac{h}{2}\left(\boldsymbol{v}_{t,i+1}+\boldsymbol{v}_{t,i}\right)\right)+\frac{1}{2}\boldsymbol{u}_{t,i}^T\frac{\partial \mathbf{K}_t(\boldsymbol{a}_{t,i})}{\partial \boldsymbol{a}_{t,i}}\boldsymbol{u}_{t,i}\right]\\
&+\frac{1}{2}\left[\left.\frac{\partial g(\boldsymbol{a}_t)}{\partial \boldsymbol{a}_t}\right|_{i+1}+\left.\frac{\partial g(\boldsymbol{a}_t)}{\partial \boldsymbol{a}_t}\right|_{i}\right]+\frac{1}{2}\left[\left.\frac{\partial \varphi(\dot{\boldsymbol{a}}_t)}{\partial \dot{\boldsymbol{a}}_t}\right|_{i+1}+\left.\frac{\partial \varphi(\dot{\boldsymbol{a}}_t)}{\partial \dot{\boldsymbol{a}}_t}\right|_{i}\right]+2\boldsymbol{\gamma}_t=0\\
&\frac{1}{2}\left[\frac{1}{2}\left(\boldsymbol{u}_{c,i}+\frac{h}{2}\left(\boldsymbol{v}_{c,i+1}+\boldsymbol{v}_{c,i}\right)\right)^T\frac{\partial \mathbf{K}_c(\boldsymbol{a}_{c,i+1})}{\partial \boldsymbol{a}_{c,i+1}}\left(\boldsymbol{u}_{c,i}+\frac{h}{2}\left(\boldsymbol{v}_{c,i+1}+\boldsymbol{v}_{c,i}\right)\right)+\frac{1}{2}\boldsymbol{u}_{c,i}^T\frac{\partial \mathbf{K}_c(\boldsymbol{a}_{c,i})}{\partial \boldsymbol{a}_{c,i}}\boldsymbol{u}_{c,i}\right]\\
&+\frac{1}{2}\left[\left.\frac{\partial g(\boldsymbol{a}_c)}{\partial \boldsymbol{a}_c}\right|_{i+1}+\left.\frac{\partial g(\boldsymbol{a}_c)}{\partial \boldsymbol{a}_c}\right|_{i}\right]+\frac{1}{2}\left[\left.\frac{\partial \varphi(\dot{\boldsymbol{a}}_c)}{\partial \dot{\boldsymbol{a}}_c}\right|_{i+1}+\left.\frac{\partial \varphi(\dot{\boldsymbol{a}}_c)}{\partial \dot{\boldsymbol{a}}_c}\right|_{i}\right]+2\boldsymbol{\gamma}_c=0
\end{aligned}
\tag{14}
$$

It could be shown that the set of equations 14 is equivalent to the stationarity conditions on the following potential function:

$$\begin{aligned}&\frac{1}{2h}\boldsymbol{v}_{i+1}^T\mathbf{M}\boldsymbol{v}_{i+1}+\frac{1}{4}\boldsymbol{v}_{i+1}^T\mathbf{C}\boldsymbol{v}_{i+1}-\frac{1}{h}\boldsymbol{v}_{i+1}^T\mathbf{M}\boldsymbol{v}_i-\frac{1}{2}\boldsymbol{v}_{i+1}\mathbf{M}\ddot{\boldsymbol{u}}_i-\frac{1}{2}\boldsymbol{v}_{i+1}^T\boldsymbol{p}_{i+1}+\frac{1}{2h}\boldsymbol{u}_{t,i}^T\mathbf{K}_t(\boldsymbol{a}_{t,i+1})\boldsymbol{u}_{t,i}+\frac{1}{2}\boldsymbol{v}_{t,i+1}^T\mathbf{K}_t(\boldsymbol{a}_{t,i+1})\left(\boldsymbol{u}_{t,i}+\frac{h}{4}\boldsymbol{v}_{t,i+1}+\frac{h}{2}\boldsymbol{v}_{t,i}\right)+\\&\frac{1}{2}\boldsymbol{v}_{t,i}^T\mathbf{K}_t(\boldsymbol{a}_{t,i+1})\left(\boldsymbol{u}_{t,i}+\frac{h}{4}\boldsymbol{v}_{t,i}\right)+\frac{1}{2h}\boldsymbol{u}_{c,i}^T\mathbf{K}_c(\boldsymbol{a}_{c,i+1})\boldsymbol{u}_{c,i}+\frac{1}{2}\boldsymbol{v}_{c,i+1}^T\mathbf{K}_t(\boldsymbol{a}_{c,i+1})\left(\boldsymbol{u}_{c,i}+\frac{h}{4}\boldsymbol{v}_{c,i+1}+\frac{h}{2}\boldsymbol{v}_{c,i}\right)+\\&\frac{1}{2}\boldsymbol{v}_{c,i}^T\mathbf{K}_c(\boldsymbol{a}_{c,i+1})\left(\boldsymbol{u}_{c,i}+\frac{h}{4}\boldsymbol{v}_{c,i}\right)+\dot{\boldsymbol{a}}_{t,i+1}^T\boldsymbol{\gamma}_t+\dot{\boldsymbol{a}}_{c,i+1}^T\boldsymbol{\gamma}_c+\frac{1}{h}\left(\eta_t\left(\boldsymbol{B}^T\boldsymbol{u}-\boldsymbol{u}_t\right)\Big|_{i+1}+\eta_c\left(\boldsymbol{B}^T\boldsymbol{u}-\boldsymbol{u}_c\right)\Big|_{i+1}+g(\boldsymbol{a}_t)|_{i+1}+g(\boldsymbol{a}_c)|_{i+1}\right)+\frac{1}{2}\left(\varphi(\dot{\boldsymbol{a}}_t)\Big|_{i+1}+\varphi(\dot{\boldsymbol{a}}_c)\Big|_{i+1}\right)\end{aligned} \tag{15}$$

Or, equivalently, to the following constrained optimization problem:

$$\begin{aligned}\min\quad&\frac{1}{2h}\boldsymbol{v}_{i+1}^T\mathbf{M}\boldsymbol{v}_{i+1}+\frac{1}{4}\boldsymbol{v}_{i+1}^T\mathbf{C}\boldsymbol{v}_{i+1}-\frac{1}{h}\boldsymbol{v}_{i+1}^T\mathbf{M}\boldsymbol{v}_i-\frac{1}{2}\boldsymbol{v}_{i+1}\mathbf{M}\ddot{\boldsymbol{u}}_i-\frac{1}{2}\boldsymbol{v}_{i+1}^T\boldsymbol{p}_{i+1}+\\&\frac{1}{2}\boldsymbol{v}_{c,i}^T\mathbf{K}_c(\boldsymbol{a}_{c,i+1})\left(\boldsymbol{u}_{c,i}+\frac{h}{4}\boldsymbol{v}_{c,i}\right)+\frac{1}{2h}\boldsymbol{u}_{c,i}^T\mathbf{K}_c(\boldsymbol{a}_{c,i+1})\boldsymbol{u}_{c,i}+\frac{1}{2}\boldsymbol{v}_{c,i+1}^T\mathbf{K}_c(\boldsymbol{a}_{c,i+1})\left(\boldsymbol{u}_{c,i}+\frac{h}{4}\boldsymbol{v}_{c,i+1}+\frac{h}{2}\boldsymbol{v}_{c,i}\right)+\dot{\boldsymbol{a}}_{c,i+1}^T\boldsymbol{\gamma}_c+\\&\frac{1}{2}\boldsymbol{v}_{t,i}^T\mathbf{K}_t(\boldsymbol{a}_{t,i+1})\left(\boldsymbol{u}_{t,i}+\frac{h}{4}\boldsymbol{v}_{t,i}\right)+\frac{1}{2h}\boldsymbol{u}_{t,i}^T\mathbf{K}_t(\boldsymbol{a}_{t,i+1})\boldsymbol{u}_{t,i}+\frac{1}{2}\boldsymbol{v}_{t,i+1}^T\mathbf{K}_t(\boldsymbol{a}_{t,i+1})\left(\boldsymbol{u}_{t,i}+\frac{h}{4}\boldsymbol{v}_{t,i+1}+\frac{h}{2}\boldsymbol{v}_{t,i}\right)+\dot{\boldsymbol{a}}_{t,i+1}^T\boldsymbol{\gamma}_t\\ s.t\\&-\dot{\boldsymbol{a}}_{t,i+1}\le 0\\&\dot{\boldsymbol{a}}_{t,i+1}\le\max\left(\frac{2}{h}\left(\boldsymbol{a}_0-\boldsymbol{a}_{t,i}\right)-\dot{\boldsymbol{a}}_{t,i},0\right)\\&-\dot{\boldsymbol{a}}_{c,i+1}\le 0\\&\dot{\boldsymbol{a}}_{c,i+1}\le\max\left(\frac{2}{h}\left(\boldsymbol{a}_0-\boldsymbol{a}_{c,i}\right)-\dot{\boldsymbol{a}}_{c,i},0\right)\\&\boldsymbol{B}^T\left(\boldsymbol{u}_{i+1}\right)-\boldsymbol{u}_{c,i+1}\ge 0\rightarrow\left(\boldsymbol{v}_{c,i+1}-\boldsymbol{B}^T\boldsymbol{v}_{i+1}\right)\le\left[\frac{2}{h}\left(\boldsymbol{B}^T\boldsymbol{u}_i-\boldsymbol{u}_{c,i}\right)+\left(\boldsymbol{B}^T\boldsymbol{v}_i-\boldsymbol{v}_{c,i}\right)\right]\\&\boldsymbol{B}^T\left(\boldsymbol{u}_{i+1}\right)-\boldsymbol{u}_{t,i+1}\le 0\rightarrow\left(\boldsymbol{B}^T\boldsymbol{v}_{i+1}-\boldsymbol{v}_{t,i+1}\right)\le\left[\frac{2}{h}\left(\boldsymbol{u}_{t,i}-\boldsymbol{B}^T\boldsymbol{u}_i\right)+\left(\boldsymbol{v}_{t,i}-\boldsymbol{B}^T\boldsymbol{v}_i\right)\right]\end{aligned} \tag{16}$$

The solution of the optimization problem 16 in each time step results the values of the state variables at the end of the time step.

It should be noted that the attained optimization problem may not be convex thus a single local minimum is not guaranteed. Hence, in case of bifurcations the question "which minimum is the one reflecting the behavior of the physical system?" may arise. Here, the insight from the physics of the problem is accounted for. Griffith's theory is based on the partial derivatives of energy quantities w.r.t the crack area. That is, Griffith's theory sets a criterion that is based on first order conditions at the current state. Hence, the correct solution is the local minimum near the current state. For the purpose of finding the solution, a gradient based approach is to be adopted. In addition, the state at the beginning of each time step should be adopted as the initial guess for the solution of the optimization problem at that time step. Moreover, a relatively small limit should be adopted to the change in the state vector in each iteration of the optimization problem.

4 EXAMPLES

4.1 SDOF system

This example considers the SDOF system presented in Figure 3. The tension spring stiffness is taken here as $k_t(a_t)=k_{0t}(a_0-a_t)^n$ while the compression spring stiffness is taken here as $k_c(a_c)=k_{0c}(a_0-a_c)^n$. The following values are assigned to the various parameters: m=1, k_{0t}=k_{0c}=2000, a_0=1.2, $2\gamma_t$=$2\gamma_c$=80, c=0. No external load was considered, however an initial velocity of 15 was accounted for. The example was executed for various values of n, namely *n=1, 2, 3, 4, 5, 10* and *20*, to explore the behavior and the stability of the algorithm. The problem is solved for a time increment of 10^{-3} and the results are summarized in Figures 5-7. Figure 5a presents the displacements of the system with various values of the exponent versus time

while Figure 5b presents the velocities. The crack area and tension stiffness versus time are presented in Figures 6a and 6b, respectively. Finally, Figure 7a presents the force-displacement relation for various values of the exponent while Figure 7b zooms on the first 1.5 time units.

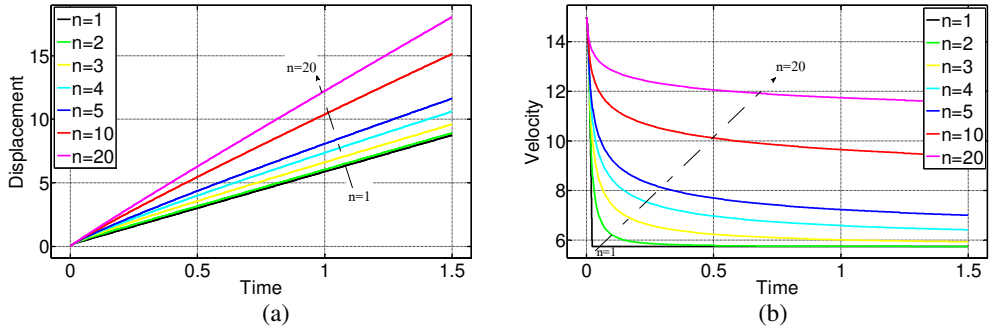

Figure 5: (a) Displacement and (b) Velocity of the mass versus time.

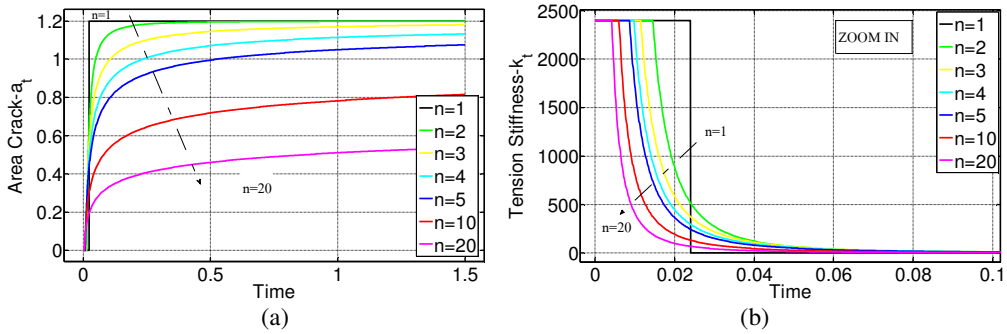

Figure 6: (a) Crack Area in tension a_t and (b) "zoom in" of Tension Stiffness k_t versus time.

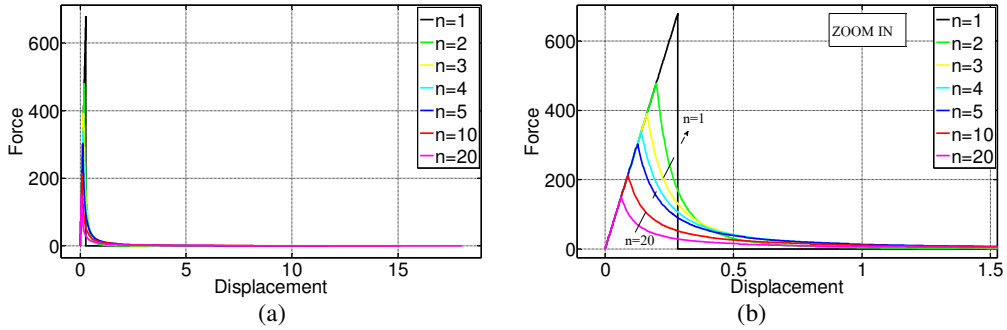

Figure 7: (a) Force-Displacement and (b) "zoom in".

It should be noted that, as expected, the area under each of the force-displacement graphs (Figure 7), that represents the spring energy, approaches $2\gamma_t \cdot a_0 = 80 \cdot 1.2 = 96$ as the crack area approaches a_0.

4.2 MDOF system

This example considers the 2 DOF system presented in Figure 8. This system is comprised of a rigid beam of mass m=1 and moment of inertia I=1 mounted on 7 systems of springs. The characteristics of all spring systems are identical. Those include a tension spring of stiffness

$k_t(a_t)=k_{0t}(a_0 - a_t)$ and surface energy $2\gamma_t$, a compression spring of stiffness $k_c(a_c)=k_{0c}(a_0 - a_c)$ and surface energy $2\gamma_c$, and a linear dashpot with a damping coefficient c. Here, $k_{0t}=k_{0c}=2000$, $a_0=1.2$, $2\gamma_t=2\gamma_c=80$, $c=0$ and $l=0.2$. No external load was considered, however an initial angular velocity of 30 was accounted for.

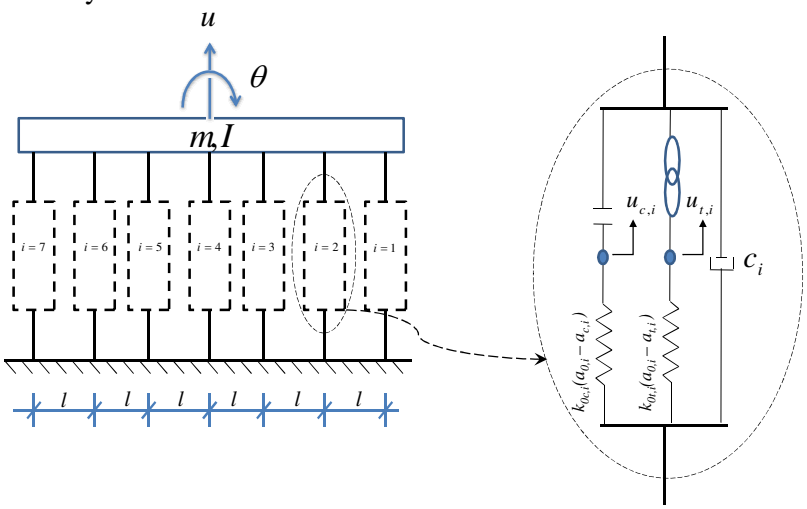

Figure 8: Two DOF system for Example 2.

The stiffness matrices for the tension-only and compression-only systems are given by:

$$\mathbf{K}_t = \begin{bmatrix} 2000\left(1.2-a_{t,1}\right) & & 0 \\ & \ddots & \\ 0 & & 2000\left(1.2-a_{t,7}\right) \end{bmatrix}$$

$$\mathbf{K}_c = \begin{bmatrix} 2000\left(1.2-a_{c,1}\right) & & 0 \\ & \ddots & \\ 0 & & 2000\left(1.2-a_{c,7}\right) \end{bmatrix}$$

Note that while those matrices look similar, they differ in the crack area variables considered. The mass and damping matrices, as well as the compatibility matrix, $\boldsymbol{B}^T$, are given by:

$$\mathbf{M} = \mathbf{I}_{2x2}$$

$$\mathbf{C} = \mathbf{0}_{2x2}$$

$$\mathbf{B}^T = \begin{bmatrix} 1 & 1 & 1 & 1 & 1 & 1 & 1 \\ -0.6 & -0.4 & -0.2 & 0 & 0.2 & 0.4 & 0.6 \end{bmatrix}^T$$

The problem is first solved for a time increment of 10^{-3} and the results are summarized in Figures 9-12. Figure 9a presents the displacements of the DOFs while Figure 9b presents their velocities. Also presented (Figures 10a and 10b, respectively) are the displacements and velocities of the connections of the springs to the beam. In addition, the tension and compression stiffnesses of the various systems are presented versus time in Figures 11a and 11b, respectively. As can be seen, during the first quarter of cycle, two pairs of springs are fractured, two in tension and two in compression. As some energy was required to result fracture, it was dissipated from the system. Hence, the total energy of the system reduced to a level such that when the direction of the angle was reversed, the potential energy was not sufficient

to result fracture. Thus, the resulted system behaves asymmetrically with reduced stiffness for rotation in one direction and full stiffness in the other. This is also reflected from Figure 10a where the time required to complete a half cycle is different in each direction.

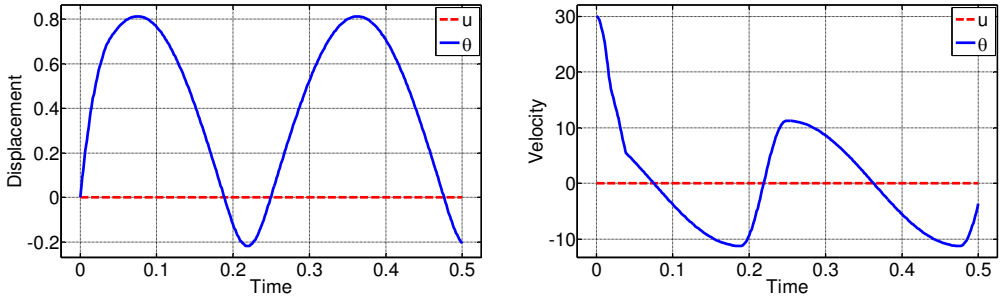

(b) (b)

Figure 9: (a) Displacement and (b) Velocity at DOFs versus time.

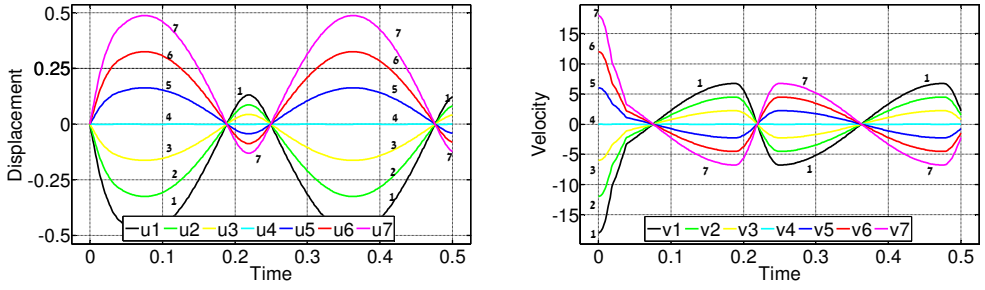

(a) (b)

Figure 10: (a) Displacement and (b) Velocity at system points (see Fig. 8) versus time.

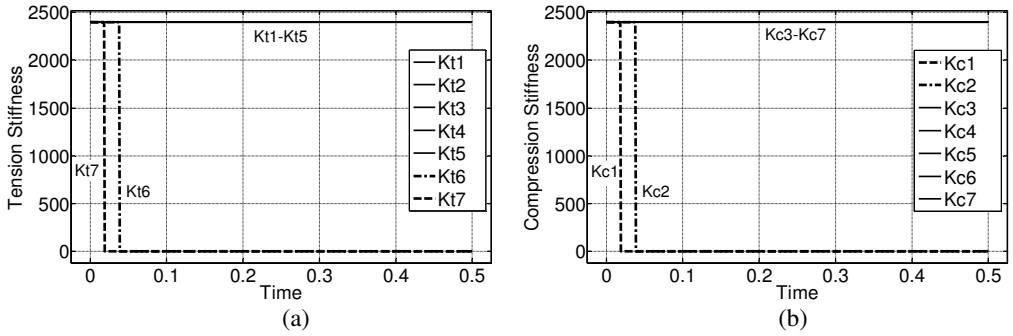

(a) (b)

Figure 11: Stiffness at (a) tension and (b) compression springs versus time.

Figures 12a and 2b present the force-displacement behavior of system 1 and 2, respectively. As can be seen, both spring present a linear relation in compression up to fracture that occurs in an instant as expected. Spring 1 fractures at time 0.019 while spring 2 fractures at time0.039 The behavior in tension remains linear as those spring systems did not fracture in tension.

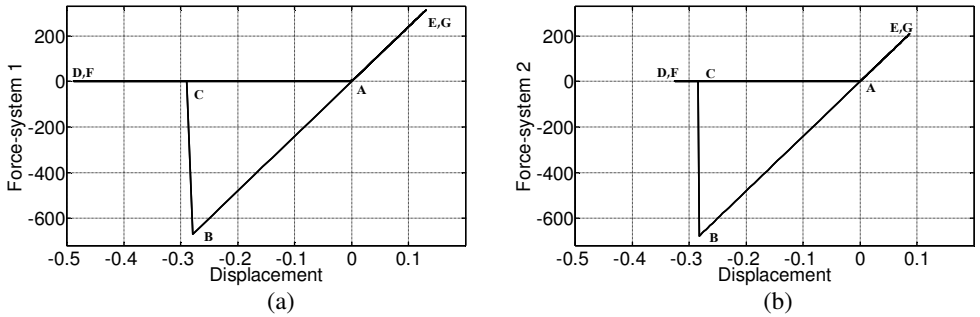

(a) (b)

Figure 12: Force-Displacement at (a) system 1 and (b) system 2

Finally, a convergence test was conducted. The problem was solved for various time increment values and the displacements and velocities of the DOFs versus time are presented in Figures 13a and 10b, respectively. Additionally, the force displacements behavior of system 1 and 2 in compression are presented in Figures 14a and 14b, respectively. As can be seen, the time increment of 10^{-3} is sufficient for convergence. This is very encouraging as the state variables of this problem show very sharp gradients in time. Those usually lead to large sensitivities. It should also be noted that while the use of a time increment of 10^{-2} leads to inaccuracy, the important phenomena are captured by the algorithm. Note also that the theoretical force and displacements of each spring at fracture are 678.82 and 0.28284, respectively. Those are traced by the algorithm with good accuracy using a time increment of 10^{-3} or smaller.

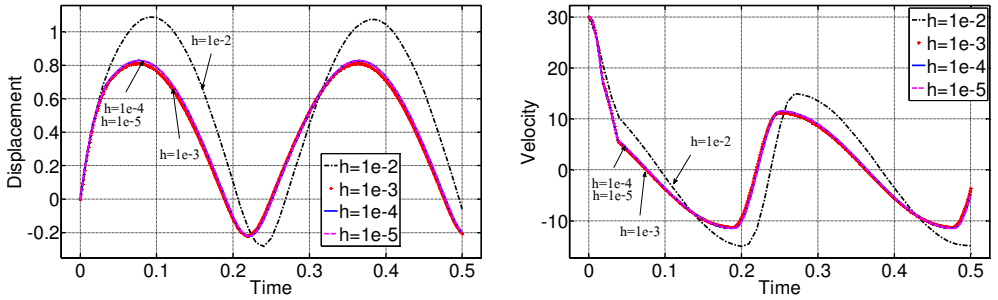

(a) (b)

Figure 13: (a) Displacements and (b) Velocities at DOFs versus time for various time increments.

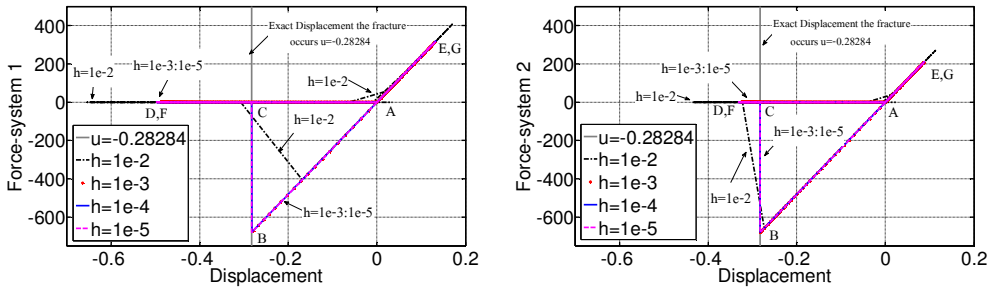

(a) (b)

Figure 14: Force-Displacement at (a) system 1 and (b) system 2 for various time increments.

5 CONCLUSIONS

- This paper presented a first step towards accounting for fracture in MLF in a unified manner through energy based fracture mechanics criteria. This important step shows feasibility of accounting for damage and fracture mechanics concepts in MLF.
- It was shown that although problems related to damage and fracture may reach bifurcation points, gained insight from the physics of the problem may assist in choosing the right path for the evolution of the state variables in time. In the problem at hand, for example, the optimization problem attained in each time step may not be convex. Nevertheless, insight from the nature of Griffith's criteria assisted in identifying the correct local minimum that, in turn, leads to the right path of the evolution in time.
- Finally, the example problems revealed that relatively large time increments were sufficient for convergence even when sudden fracture (n=1) was considered. This is very encouraging and is attributed to the weak formulation in time.

6 ACKNOWLEDGEMENT

This research was supported by a Grant from the G.I.F., the German-Israeli Foundation for Scientific Research and Development. The authors gratefully acknowledge this support.

REFERENCES

[1] U. Starossek, *Progressive Collapse of Structures.* Thomas Telford Publishing, 2009.

[2] A. J. Pretlove, M. Ramsden, A.G. Atkins, Dynamic effects in progressive failure of structures. *International Journal of Impact Engineering* **11**(4): 539-546, 1991.

[3] G. Kaewkulchai, and E.B. Williamson, Beam element formulation and solution procedure for dynamic progressive collapse analysis. *Computers and Structures* **82**: 639-651, 2004.

[4] R. Villaverde, Methods to assess the seismic collapse capacity of building structures: State of the art. *Journal of Structural Engineering* **133**(1): 57-66, 2007.

[5] D. Isobe, and M. Tsuda, Seismic collapse analysis of reinforced concrete framed structures using the finite element method. *Earthquake Engineering & Structural Dynamics* **32**: 2027–2046, 2003.

[6] M. Hakuno, K. Meguro, Simulation of Concrete-Frame Collapse due to Dynamic Loading. *Journal of Engineering Mechanics* **119**(9): 1709-1723, 1993.

[7] Z.P. Bazant, and M. Verdure, Mechanics of progressive collapse: learning from world trade center and building demolitions. *Journal of Engineering Mechanics, ASCE*, **133**(3), 308-319, 2007.

[8] B.A. Izzuddin, A.G. Vlassis, A.Y. Elghazouli, D.A. Nethercot, Progressive collapse of multi-storey buildings due to sudden column loss -Part I: Simplified assessment framework. *Engineering Structures,* **30** :1308–1318, 2008.

[9] S.K. Kunnath, A.M. Reinhorn, J.F. Abel, A Macromodel Approach to Practical Analysis of R/C Buildings under Seismic Excitation*, in Computer Aided Analysis and Design of Concrete Structures, N. Bicanic and H. Mang (Eds.), Pineridge Press, Vol. 2*, 1155-1167, 1990.

[10] Y. Bao, S.K. Kunnath, S. EL-Tawil, H.S. Leo, Macromodel-based simulation of progressive collapse: RC frame structures. *Journal of Structural Engineering, ASCE,* **134** (7): 1079-1091, 2008.

[11] L.F. Ibarra, R.A. Medina, H. Krawinkler, Hysteretic models that incorporate strength and stiffness deterioration. *Earthquake Engineering and Structural Dynamics*, **34**(12), 1489-1511, 2005.

[12] K.J. Elwood and J.P. Moehle, Dynamic collapse analysis for a reinforced concrete frame sustaining shear and axial failures. *Earthquake Engineering and Structural Dynamics*, **37**(7), 991-1012, 2008.

[13] J.E. Rodgers, S.A. Mahin, Effects of Connection Fractures on Global Behavior of Steel Moment Frames Subjected to Earthquakes*. Journal of Structural Engineering*, **132**(1), 78-88, 2006.

[14] D.E. Grierson, L. Xu, Y. Liu, Progressive-Failure Analysis of Buildings Subjected to Abnormal Loading. *Computer-Aided Civil and Infrastructure Engineering*, **20**(3), 155-171, 2005.

[15] D. Hartmann, M. Breidt, V.V. Nguyen, F. Stangenberg, S. Hohler, K. Schweizerhof, S. Mattern, G. Blankenhorn, B. Moller, M. Liebscher, Structural collapse simulation under consideration of uncertainty - Fundamental concept and results*. Computers & Structures* **86**(21-22): 2064-2078, 2008.

[16] M.V. Sivaselvan, A.M. Reinhorn, Lagrangian approach to structural collapse simulation. *Journal of Engineering Mechanics, ASCE*, **132** (8): 795-805, 2006.

[17] L. Meirovitch, *Methods of analytical dynamics*. McGraw-Hill, 1970.

[18] B. Halphen, Q.S. Nguyen, Sur les materiaux standard generalizes. *Journal de Mecanique* **14**(1): 39, 1975.

[19] M.V. Sivaselvan, O. Lavan, G.F. Dargush, H. Kurino, Y. Hyodo, R. Fukuda, K. Sato, G. Apostolakis, A.M. Reinhorn, Numerical collapse simulation of large-scale structural systems using an optimization-based algorithm. *Earthquake Engineering & Structural Dynamics*, **38**(5): 655-677, 2009.

[20] O. Lavan, Dynamic analysis of gap closing and contact in the Mixed Lagrangian Framework – towards progressive collapse prediction. *Journal of Engineering Mechanics, ASCE*, **136**(8), 979-986, 2010.

[21] O. Lavan, M.V. Sivaselvan, G.F. Dargush, Progressive collapse analysis through

strength degradation and fracture in the Mixed Lagrangian Framework. *Earthquake Engineering & Structural Dynamics*, **38**(13): 1483-1504, 2009.

[22] T.L. Anderson, *Fracture Mechanics: Fundamentals and Applications*. CRC Press, 1995.

[23] A.A. Griffith, The phenomena of rupture and flow in solids. *Philosophical Transactions of the Royal Society of London,* **A221**: 163–198, 1921.